Journal of Materials Chemistry C

ROYAL SOCIETY OF CHEMISTRY

PAPER

View Article Online
View Journal | View Issue

Cite this: J. Mater. Chem. C, 2023, 11, 16982

New RM734-like fluid ferroelectrics enabled through a simplified protecting group free synthesis†

Calum J. Gibb *[a] and Richard J. Mandle [ab]

Received 30th August 2023,
Accepted 22nd November 2023

DOI: 10.1039/d3tc03134a

rsc.li/materials-c

We report a novel and simplified synthetic procedure for making analogues of the widely studied ferroelectric nematogen **RM734**. Our new procedure focuses on building materials starting from the nitro-terminus and eschewing protecting groups, in contrast to previously reported syntheses. This new synthetic approach confers two principal advantages: firstly, the synthesis of the variants described herein is expedient, being a single step as opposed to three or more *via* the classical route. Secondly, by forgoing the use of benzyl groups as utilised in the original synthesis we can include functionality that is incompatible with hydrogenolysis conditions (*e.g.* olefins, late halogens, unsaturated heterocycles). Several of the **RM734**-like materials we report exhibit ferroelectric nematic phases, and we rationalise the behaviour of these materials with aid of electronic structure calculations, potential energy surface scans and atomistic molecular dynamics simulations.

Introduction

Nematic liquid crystals possess a degree of orientational order of their constituent molecules (or particles) along a direction termed the director ($\hat{n}$) and are widely exploited in display technology. It had long been considered that nematic (N) phases, even when comprised of extremely polar molecules, do not show a preference for bulk polar order; the molecular electric dipole vectors have an equal probability of orientation parallel or antiparallel with the director (*i.e.* $\hat{n} = -\hat{n}$, Fig. 1a). A nematic phase with polar ordering would also be ferroelectric; having the vast majority of its constituent electric dipole moments oriented along a single direction ($-\hat{n} \neq -\hat{n}$, Fig. 1b). In 2017 Mandle *et al.*[1] and Nishikawa *et al.*[2] simultaneously and independently reported highly polar liquid crystalline materials that exhibited multiple nematic phases. The lower temperature nematic phase is now understood to be polar and is termed the ferroelectric nematic (N_F) phase. The N_F phase is of special scientific interest[3–12] due to the presence of polar order in a fluid system coupled with a strong linear electrooptical response[13,14] and large polar domains.[15] The N_F phase may also be aligned using existing alignment techniques originally developed for conventional nematics,[16] and potential applications are beginning to emerge, including photo-variable capacitors[17] and electrostatic actuators.[18]

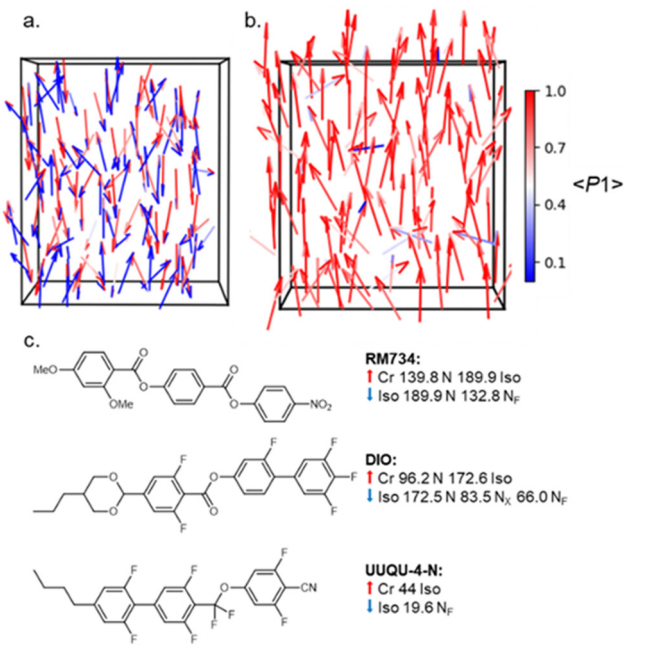

Fig. 1 Molecular organization in the apolar nematic (a) and ferroelectric nematic (b) phases; arrows represent molecular electric dipole moments and are coloured according to the polar order parameter $\langle P1 \rangle$ which takes a value of 0.06 in (a) and 0.89 in (b), while $\langle P2 \rangle$ is ~0.65 in both cases. (c) The molecular structures and transition temperatures (°C) of the three of the archetypal ferroelectric nematogens: **RM734**,[1] DIO,[2] and UUQU-4-N.[19]

[a] School of Chemistry, University of Leeds, Leeds LS2 9JT, UK. E-mail: c.j.gibb@leeds.ac.uk
[b] School of Physics and Astronomy, University of Leeds, Leeds LS2 9JT, UK

† Electronic supplementary information (ESI) available. See DOI: https://doi.org/10.1039/d3tc03134a

Despite a growing number of reported materials which exhibit the N_F phase (for example[20–29]) studies into the phase are still in their infancy and little is known about how certain structural features drive N_F phase formation. As a result, the majority of reported ferroelectric nematogens can be broadly classed as derivatives of one of the three archetypal structures (Fig. 1c): **RM734**,[1] DIO[2] and UUQU-4-N.[19] For **RM734**, the synthesis is typically performed left-to-right, installing the 4-nitrophenyl unit last and employing a benzyl protecting strategy (Fig. 2(a)). The benzyl group enables high yields, but the hydrogenolysis deprotecting step brings issues of functional group compatibility. An alternative synthetic strategy has using a tetrahydropyranyl protecting group,[21] suffers from low yields (Fig. 2(b), *circa* 40% over 3 steps). Herein we report a new synthetic pathway to '**RM734**-like' compounds which installs the aromatic rings in the opposite order to the original synthesis of **RM734** right-to-left (Fig. 3(d)). We eschew the need for any protecting groups entirely and allows for the highest possible functional group compatibility. We utilize this new methodology to report a series of novel **RM734** derivatives, including those with halogens and alkenes at the terminus, some of which exhibit the N_F phase.

Experimental

Unless otherwise noted, all chemicals were purchased from commercial suppliers and used as received. Solvents were purchased from Merck. Reactions were monitored by TLC using UV light (254 nm). Chromatographic purification was performed using a Combiflash NextGen 300+ system (Teledyne Isco) using silica gel cartridges as the stationary phase and a hexane/DCM gradient as the mobile phase. The chromatographed materials were then recrystallized from the indicated solvent system, collected by filtration, and dried under reduced pressure. The materials were characterised by ^{1}H, ^{13}C{^{1}H} and, where appropriate, ^{19}F NMR. Electronic structure calculations were performed with the B3LYP hybrid functional and the LAN2DZ basis set[32] in Gaussian G09 revision D01.[33] Bimolecular PES scans employed additional GD3BJ dispersion[34] and counterpoise correction terms. Following geometry optimisation we performed a frequency calculation, with the absence of imaginary frequencies taken to indicate the optimisation was at a minimum. We generated electrostatic potential (ESP) isosurfaces using the Gaussian formchk and cubegen utilities; the resulting cube files were then rendered using VMD. The interactions strength was quantified by performing a relaxed potential energy scan of the separation between two molecules arranged head-to-tail, from an initial separation of 2.5 Å to a maximum of 7 Å in 0.1 Å steps. Full experimental details, including synthetic procedures, structural characterisation and purity analysis are provided in the ESI.†[34]

Results and discussion

The previously reported synthesis of **RM734** employs a benzyl (OBn) protecting strategy, beginning from 2,4-dimethoxybenzoic acid and eventually affording the title compound in high yield over three linear steps (Fig. 2(a)). The nitrophenyl unit is installed last, owing to the incompatibility of this group with the hydrogenolysis conditions employed for debenzylation. Saha *et al.* have also reported a four-step synthetic pathway to the synthesis of **RM734**-like materials in which they forgo the use of the OBn protecting group, by instead obtaining the acid *via* aldehyde oxidation prior to the final esterification.[35] Li *et al.*[24] and Stepanafas *et al.*[31] instal the ring units of **RM734** in reverse order (Fig. 2(b)); utilising a tetrahydropyranyl (THP) protecting group to synthesise 4-nitrophenyl 4-hydroxybenzoate and similar derivatives in ∼ 40% yield, this then being subjected to terminal esterification to afford **RM734**. The modest yields afforded using this method are likely due to issues regarding chemical selectivity due to the presence of both the phenolic and acidic moieties as well as issues associated with cleavage of the group during purification by SiO_2 gel chromatography as the group is easily cleaved under mildly acidic conditions.[36] This makes the THP group non-ideal for in the case of the synthesise of **RM734**.

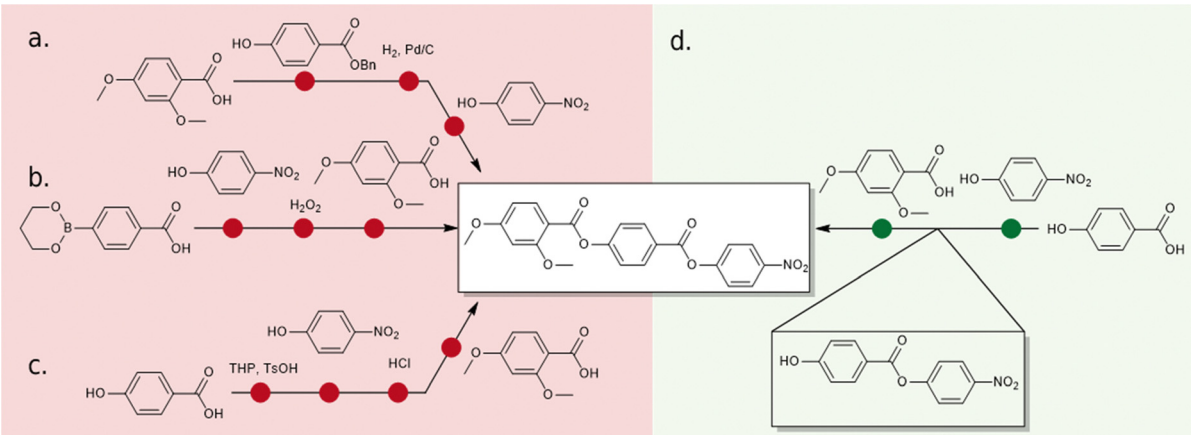

Fig. 2 (a) Original synthesis of **RM734** reported by Mandle *et al.*,[1] (b) synthesis of **RM734** and related materials reported Kumar *et al.*;[30] (c) the synthetic route reported by Li *et al.*[24] and Stepanafas *et al.*[31] which employs the use of the THP protecting group; and (d) synthetic route developed and used in this work.

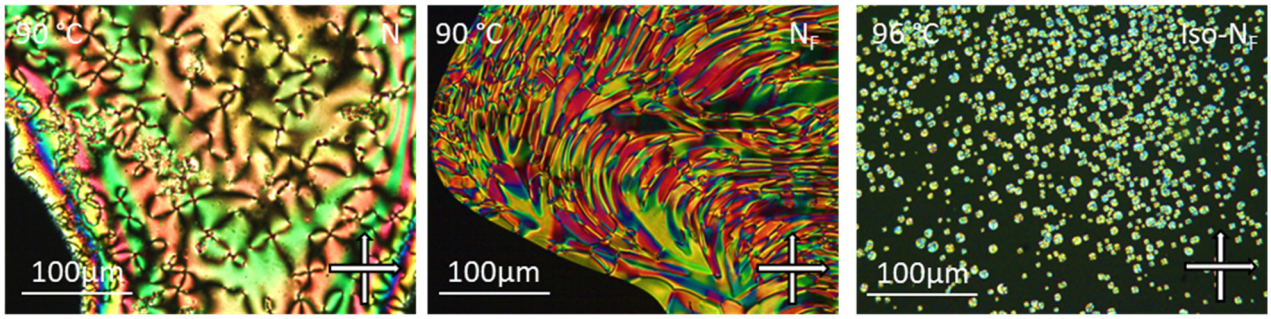

Fig. 3 A nematic Schlieren texture containing both 2- and 4-point brush defects observed for compound **4** (a), an example of the banded texture of the N_F phase observed for compound **3** (b), and the growth of point singularities at the I–N_F phase transition observed on cooling for compound **2** (c). All textures were observed between untreated glass slides.

Kumar *et al.* have also employed a synthetic strategy in which the rings are installed in the reverse order.[30] The method presented by Kumar *et al.* contains only three synthetic steps using a boronic ester as the protecting group (Fig. 2(c)). Whist containing only three-synthetic steps from the boronic ester, the group is hydrolytically labile which may lead to unwanted side reactions occurring.

Our initial synthetic effort was to focus on improving this yield by utilizing a tert-butyldimethylsilyl (TBDMS) protecting group. Regrettably, the TBAF mediated cleavage invariably led to significant ester hydrolysis and this method was promptly abandoned as unworkable due to the lability of the 4-nitrophenyl group. We found success by avoiding protecting groups entirely (Fig. 2(d)). Our initial hint was that esterification of 4-hydroxybenzoic acid and 4-nitrophenol in a 1 : 1 ratio on a mmol scale gave good conversion to the desired product. As had been previously reported however, separation by standard re-crystallisation techniques from residual 4-nitrophenol was challenging.[37–39] Gratifyingly, large scale attempts using a 1 : 2 mixture of 4-hydroxybenzoic acid and 4-nitrophenol reacted equally smoothly under Steglich conditions with EDC/DMAP which was successfully purified by flash chromatography using a gradient elution of Hexane/DCM to afford the title compound in 55% yield in a single step. After chromatography, we note that the material is somewhat unstable on silica which explains the modest yield achieved however, this instability is relieved following subsequent esterification. Subsequent Steglich esterification of 4-nitrophenyl 4-hydroxybenzoate with a library of substituted benzoic acids afforded compounds 1–11 in moderate to good yield (67–88%) in a method ultimately requiring only two synthetic steps.

We first synthesised five **RM734**-analogues which have various modifications made to the 2,4-dimethoxybenzoate unit. Transition temperatures and phase assignments (made *via* polarized optical microscopy (POM)) for compounds **1–5** are given in Table 1. The conventional N phases are assigned based upon the observation of characteristic Schlieren textures containing 2- and 4-point brush singularities (Fig. 3(a)). The N_F phases have been assigned based on the observation of a banded textures (Fig. 3(b)), now thought to be characteristic

Table 1 Transition temperatures (T, °C) and associated enthalpies (ΔH, kJ mol^{-1}) for compounds **1–5**?

No.	R =		Melt	N_F–N/Iso	N–Iso
RM734	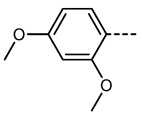	*T*	139.8	132.7	187.9
		ΔH	34.8	0.20	0.60
1	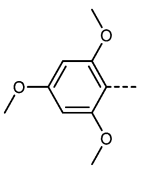	*T*	181.9	—	—
		ΔH	43.0	—	—
2	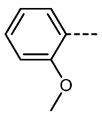	*T*	136.4	96.3	—
		ΔH	32.9	1.7	—
3	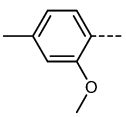	*T*	157.3	125.0	151.6
		ΔH	32.2	1.0	0.5
4	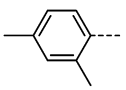	T	151.1	—	182.0
		ΔH	36.8	—	0.5
5	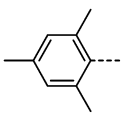	T	137.8	—	119.8
		ΔH	38.7	—	0.3

of the phase.[24,28,40] In cases where a direct N_F–isotropic(I) phase transition is observed, the N_F phase is seen to grow from point singularity defects (Fig. 3(c)) which coalesce to form the characteristic bulk texture. This observation has been reported previously for the N_F–I transition.[19,41] To further affirm the assignments of the N_F phase, binary mixtures of the ferroelectric nematogens and **RM734** have been prepared showing good miscibility across all concentrations. The N_F phase is observed for all concentrations studied with an approximately linear dependence of the transition temperatures. The phase diagram for 2/**RM734** is presented in Fig. 4 (top) whilst the data for other materials is given in the ESI† to this article. Calculated

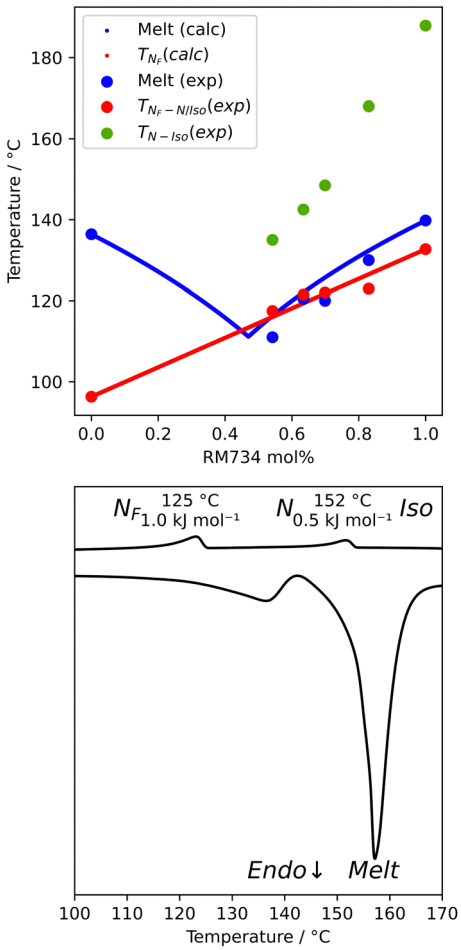

Fig. 4 Phase diagram constructed by mixing **2** and **RM734** (top), and DSC thermogram for compound **3** showing the N–I and N_F–N phase transitions (bottom).

phase diagram data (melting points, transition temperatures) were obtained using data from DSC experiments on pure materials using the *Eutectic* software tool.[42] The transition temperatures and associated enthalpy changes are extracted from their respective DSC thermograms (for example Fig. 4 (bottom)), measured at a heat/cool rate of 20 °C min^{-1} under a nitrogen atmosphere.

Compared to **RM734**, compound **1** has an additional OMe group in the 6-position and this sees a significant increase in the melting point and the total loss of mesogenic behaviour. Contrast this with the removal of the terminal methoxy group (4-position) of **RM734**; this gives compound **2** material, which exhibits a direct N_F–Iso transition (albeit with an onset below that of the parent material) as well as a small reduction in melting point. This suggests that, whilst a terminal chain is beneficial for 'classical' non-polar nematics, it is not a requirement for the polar N_F phase; and indeed the deleterious effect of long terminal chains on the stability of the N_F phase is well known.[25,27,28,40,43,44] Crudely put, this reflects the origins of the N_F phase being in electrostatic (dipole–dipole) forces, whereas the conventional nematics result from shape anisotropy.

We next study the loss of oxygen atoms from the terminal/lateral methoxy group(s) of **RM734** and compound **1**. Compound **3**, in which the terminal (4-) methoxy group is replaced with a methyl group has only a modest reduction in T_{NF-N}, a sharp reduction in T_N–Iso and a modest increase in melting point. Compound **4** is closely related to **3**, having both the terminal and lateral methoxy groups replaced with methyl; however, the mesomorphic behaviour of **4** is rather different, with this material only exhibiting a conventional nematic phase. To a first approximation, this can be understood to be a consequence of the reduced dipole moment that results from the loss of the lateral methoxy group, and we will demonstrate this shortly (*inter alia*). In **5** we add an additional methyl group to **4** in the 2-position (or alternatively, we replace the methoxy units of **1** with methyl); with the resulting material exhibiting a conventional nematic phase.

We optimised the geometries of **RM734** and compounds **1–5** at the B3LYP/LAN2LDZ level of DFT in order to rationalise the trends in observed mesophase behaviour (Table 2). Compound **1** is non mesogenic, despite being of comparable electrical polarity to **RM734**. In **1** the additional breadth that results from the two lateral methoxy units is reflected in a low value of the shape anisotropy parameter (ShAP). Compounds **2** and **3** both exhibit the N_F phase, albeit at reduced temperature to the

Table 2 Properties from DFT calculations on **RM734** and compounds **1–5**: molecular electric dipole moment (μ, Debye); anisotropy of polarizability ($\Delta\alpha/Å^3$); Shape Anisotropy Parameter (ShAP), defined here as $l/\sqrt{(wb)}$, where $l/w/b$ are the molecular length, width, and breadth, respectively; Rotational Anisotropy Parameter (RotAP) defined here as $R_1/\sqrt{(R_2R_3)}$, where $R_{1/2/3}$ are the rotational constants

No.	R =	μ/D	$\Delta\alpha/Å^3$	ShAP	RotAP
RM734	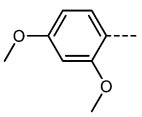	12.78	51.1	4.8	21.1
1	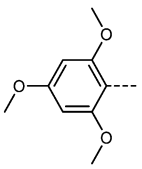	12.23	46.2	3.5	21.0
2	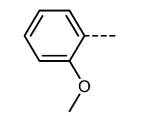	11.55	43.8	4.6	18.9
3	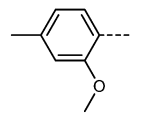	12.46	47.6	4.6	19.8
4	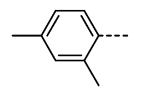	10.65	47.9	5.7	19.9
5	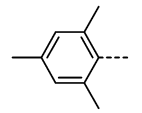	9.88	46.6	3.9	19.8

parent; they have comparable electric dipole moments to **RM734**, as well as being sufficiently anisotropic in shape to permit the formation of mesophases. Compounds **4** and **5** lack the lateral methoxy unit, and as such exhibit notably reduced electric dipole moments which are perhaps below the threshold required to exhibit the N_F phase in this system. This result demonstrates the apparent necessity of the lateral methoxy group in promoting N_F behaviour in **RM734**-like materials.

The inclusion of late-halogen atoms in **RM734** is complicated by the prior use of hydrogenolysis, with these often being labile under the H_2/Pd conditions employed. Our new synthetic approach makes the inclusion of halogen atoms on the -left- and central-rings synthetically straightforward. To demonstrate this, we elected to synthesis compounds **6–9** which contain I, Br, Cl and, F, respectively, in the 4-position on the left-hand ring. The transitional temperatures and phase assignments of these compounds are shown in Table 3. Halogen atom are known for their ability to exhibit Sigma-holes,[45,46] as well as being able to partake in a wide range of synthetic transformations.

All the halogen terminated homologues exhibit monotropic nematic phases with only the iodine terminated derivative exhibiting the N_F phase (Fig. 5). The values of T_{N-I} remain almost constant for the three largest halogens, with a significant decrease observed for the fluorine terminated derivative. We optimised the geometries of **RM734** and compounds **6–9** at the B3LYP/LAN2LDZ level of DFT in order to rationalise the trends in observed mesophase behaviour (Table 4). Immediately it is clear that a halogen atom at the 4-position leads to the expected reduction in molecular electric dipole moment relative to the parent **RM734**. The shape anisotropy parameter is almost constant across this series, while the rotational anisotropy parameter follows the expected trend as a consequence of the large mass of the halogen atom.

Table 3 Transition temperatures (T, °C) and associated enthalpies (ΔH, kJ mol^{-1}) for compounds **6–9**

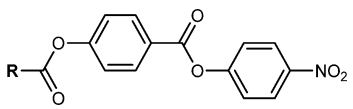

No.	R =		Melt	N_F–N/Iso	N–Iso
6	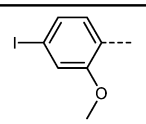	T	187.7	106.5[a]	147.5
		ΔH	39.8	—	0.8
7	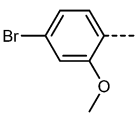	T	180.0	—	155.7
		ΔH	44.9	—	0.7
8	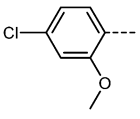	T	173.6	—	150.5
		ΔH	43.2	—	0.7
9	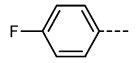	T	172.0	—	125.9
		ΔH	43.2	—	0.5

[a] Temperature given based upon POM observations.

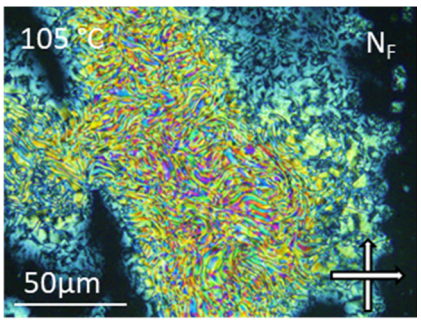

Fig. 5 The banded texture observed by POM between untreated glass slides for the N_F phase of compound **6** at 105 °C.

Table 4 Properties from DFT calculations on RM734 and compounds 6–9 molecular electric dipole moment (μ, Debye); anisotropy of polarizability ($\Delta\alpha$/Å^3); Shape Anisotropy Parameter (ShAP); Rotational Anisotropy Parameter (RotAP)

No.	R =	μ/D	$\Delta\alpha$/Å^3	ShAP	RotAP
RM734	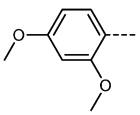	12.78	51.1	4.8	21.1
6	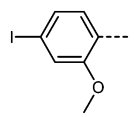	9.83	55.9	4.8	19.9
7	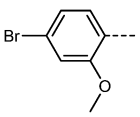	9.40	52.2	4.8	19.7
8	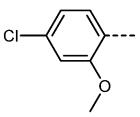	9.04	49.2	4.8	19.6
9	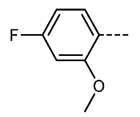	9.01	44.4	4.7	19.1

It is somewhat surprising that the iodo-terminated **6** exhibits the N_F phase, while **7–9** do not; we therefore computed the molecular electrostatic potential on the 0.001 au electron density for each of these compounds (and also **RM734**). The ESP isosurface of **RM734** is as expected, with the nitro- and carboxylate-groups giving rise to regions of enhanced electron density. Materials incorporating a terminal iodo-group feature a large Sigma hole – a region of positive charge which can partake in non-covalent interactions – with a smaller feature being seen for the bromo- terminated material (shown in Fig. 6a and c). For the fluoro- and chloro- terminated materials we do not find such a feature. Experimentally, the observation of an N_F phase for the iodo-terminated materials suggests a propensity for head-to-tail ordering which implies the existence

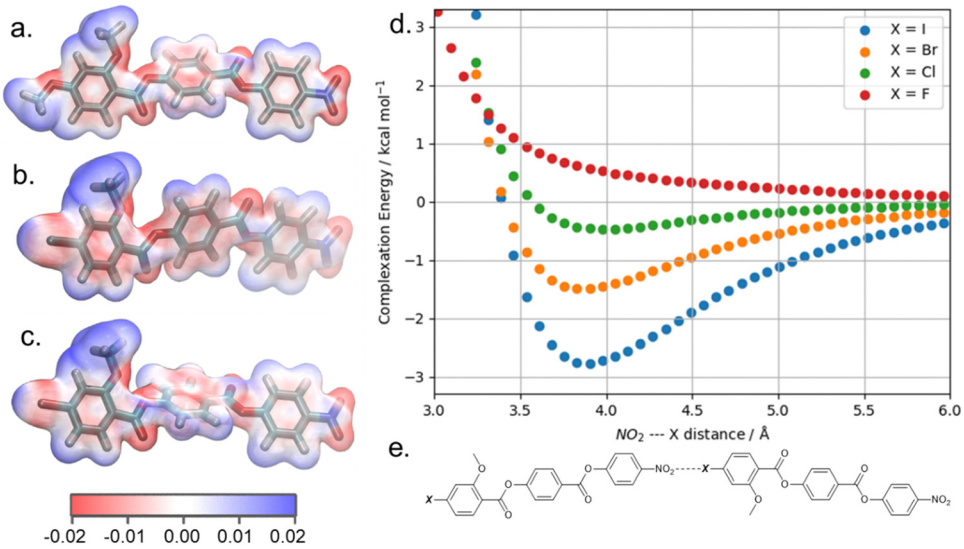

Fig. 6 Optimized geometries of **RM734** ((a) –OMe terminus), **6** ((b) –I terminus), **7** ((c) –Br terminus), at the B3LYP-GD3BJ/LAN2DZ level of DFT, with the electrostatic potential (ESP, isovalue = 0.04 a.u.) on the 0.001 au electron density isosurface. (d) Complexation energy (kcal mol^{-1}) as a function of nitro-'X' separation (Å) for homodimers of compounds **6–9** (X = I, Br, Cl, F) as computed at the B3LYP-GD3BJ/LAN2DZ level of DFT; (e) diagram illustrating the distance referenced in (d) for a homodimer.

of electrostatic interactions between the terminal group and the nitro group at the other terminus.

To quantify the potential for interactions between these groups we performed potential energy scans for head-to-tail homodimers of **RM734**, and compounds **6–9** Our calculations employ the B3LYP hybrid functional, GD3BJ dispersion correction, the LAN2DZ basis set, and additional counterpoise correction. We start from a homodimer of each compound, with the Ph-NO_2 and Ph-X bonds – where X is OMe, F, Cl, Br, or I – being oriented on the same vector and with a separation of 2.5 Å between the nitro and X groups, and increase the separation in 0.1 Å steps.

We compute the complexation energy as function of the distance between the nitro group and the terminal group in question by performing relaxed scans about the potential energy surface (Fig. 6d). The iodo terminated material **6** has the largest Sigma hole and this displays a large complexation energy (~2.7 kcal mol^{-1}) at a separation of 3.7 Å. In contrast, the bromo-terminated material has a much smaller complexation energy (~1.3 kcal mol^{-1}) and the chloro- is smaller still (~0.4 kcal mol^{-1}). Owing to the electronegativity of its terminal fluorine group, **9** experiences electrostatic repulsion (*i.e.* positive complexation energy).

The final compounds we elected to synthesise using our new synthetic approach are compounds **10** and **11**. Like the halogen containing compounds discussed previously, both compounds are reactive under the hydrogenolysis conditions previously employed in the synthesis of **RM734** making them difficult if not impossible to obtain using the previously reported methodologies. The transitional temperatures of compounds **10** and **11** are shown in Table 5. Compound **10** may be compared to the parent **RM734** molecule with an additional olefin inserted between the ester-link and left-hand ring. Inclusion of the unsaturated moiety significantly increases the melting point and N–I transition temperature and sees the extinction of the N_F phase. The increase in melting point and isotropisation temperature probably results from both the increased molecular length and the enhanced intermolecular interactions (relative to **RM734**) that result from incorporation of the cinnamate unit. The short range of supercooling precludes the observation of a monotropic N_F phase. Compound **11** shows an enantiotropic N_F phase which transitions directly into the isotropic phase, as determined by POM (Fig. 7). As will be shown shortly, the later is probably a consequence of increased electric dipole moment.

We optimised the geometries of **RM734** and compounds **10** and **11** at the B3LYP/LAN2LDZ level of DFT (Table 6). Utilisation of the cinnamate ester in **10** leads to an increase in molecular

Table 5 Transition temperatures (T, °C) and associated enthalpies (ΔH, kJ mol^{-1}) for compounds **10** and **11**

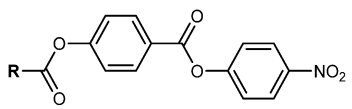

No.	R =		Melt	N_F–N/Iso	N–Iso
10	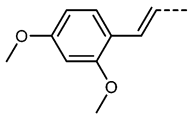	T	173.2	—	251.8
		ΔH	38.6	—	1.5
11	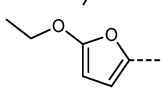	T	191.4	205.0[a]	—
		ΔH	32.4	—	—

[a] Temperature given based upon POM observations as it is not observed by DSC at 20 °C min^{-1}.

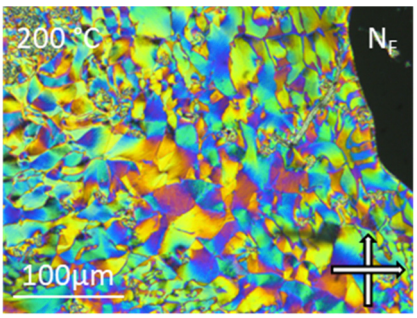

Fig. 7 The banded texture observed by POM between untreated glass slides for the N_F phase of compound **11** at 200 °C.

Table 6 Properties from DFT calculations on **RM734** and compounds **10–11** molecular electric dipole moment (μ, Debye); anisotropy of polarizability ($\Delta\alpha$/Å^3); Shape Anisotropy Parameter (ShAP); Rotational Anisotropy Parameter (RotAP)

No.	R =	μ/D	$\Delta\alpha$/Å^3	ShAP	RotAP
RM734	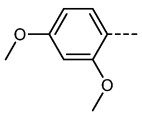	12.78	51.1	4.8	21.1
10	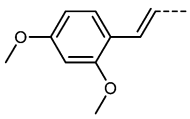	14.74	68.9	6.8	23.5
11	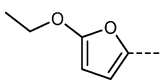	13.22	46.0	5.1	18.8

length; in turn, this gives a larger electric dipole moment (as a consequence of the larger separation of charges) and larger values of ShAP/RotAP. Under experimental conditions **10** does not exhibit the N_F phase, rather it crystallises on cooling prior to reaching this point. In compound **11** the presence of the 2-ethoxyfuran unit leads to a slightly larger electric dipole moment than the parent material which, *inter alia*, leads to a direct N_F–Iso transition at high temperature, beyond even the isotropisation temperature of the parent material. The high melting point of **11** defied our expectations that the bent ($\sim$120°) geometry of this unit would lead to a 'low' melting point, nevertheless the high T_{NF-N} is a welcome observation.

Experimentally, compound **11** shows low solubility in with other N_F materials and so we are unable to confirm the phase identification through binary mixtures or contact preparations. Compound **11** also begins to degrade above its melting point, making detailed physical study complicated, and so we consider the phase assignment as N_F to be tentative. We therefore opted to explore the unusually high T_{NF-Iso} in this material computationally, through the use of fully atomistic molecular dynamics simulations. Full details on simulation setup and parametrisation are given in the ESI† to this article; briefly, simulations comprised 600 molecules of **11**, and commenced from a polar nematic starting configuration and at various temperatures with a production MD run of 250 ns. Our MD

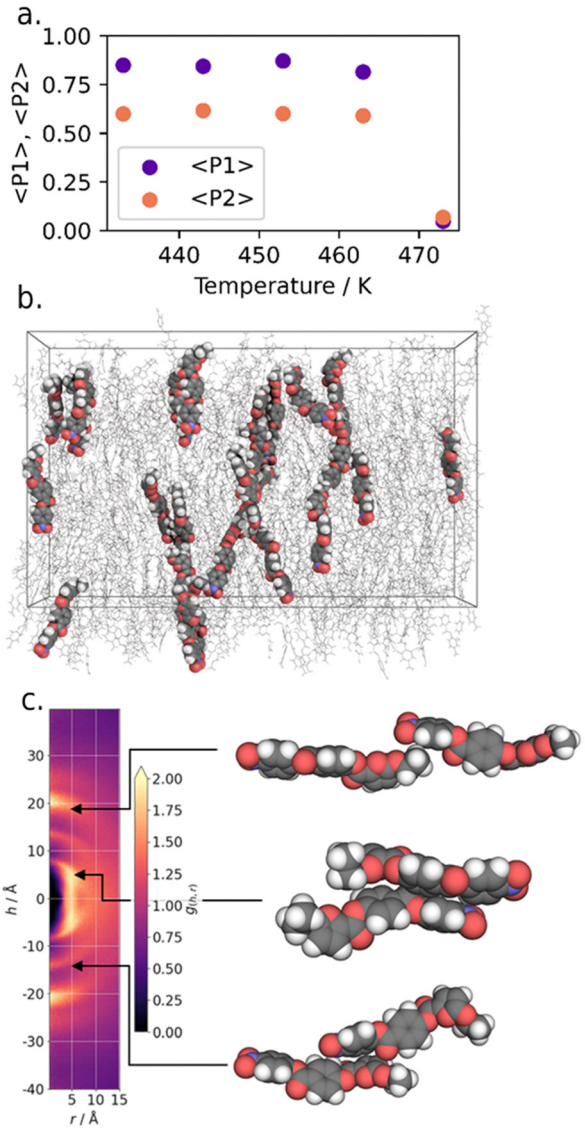

Fig. 8 (a) plot of the polar ($\langle P1\rangle$) and orientational ($\langle P2\rangle$) order parameters as a function of simulation temperature for fully atomistic MD simulations of **11**. (b) Instantaneous configuration of the polar (N_F) nematic configuration of **11** at a temperature of 443 K (170 °C) at a simulation time of 231 ns. Molecules are shown as wireframe with 25 randomly selected and shown as space filling. (c) Cylindrical distribution function (CDF) of the polar (N_F) nematic configuration of **11** at a temperature of 413 K (140 °C).

simulations appear to underestimate the experimental clearing point by 10–20 °C; at and below temperatures of 463 K we find polar nematic order to be stable, although the values of $\langle P1\rangle$ we obtain are persistently lower than those obtained under the same methodology for **RM734**, DIO, and UUQU-4-N (Fig. 8(a)).[4,43]

We gained additional insight by examination of the cylindrical distribution function of the MD trajectory (Fig. 8(c)). On-axis arcs centred at $h = \pm 20$ Å result from head-to-tail pairing, whereas additional arcs at $h \sim \pm 14$ Å and ± 9 Å result from close contacts between the furan ring and carboxylate esters on adjacent molecules. Our interpretation of this data is that the localised electron density that results from the furan-ring

enables and favours stronger electrostatic interactions between adjacent molecules, and experimentally this manifest as a large increase in $T_{NF\text{-}I}$. We consider that other related heterocyclic systems (*e.g.* oxazoles, thiazoles) may allow us to take advantage of these favourable interactions without incurring such a heavy penalty in terms of melting point. This now requires further study.

Conclusions

We report a new route to synthesise **RM734** and derivatives which forgoes protecting groups entirely and offers expedient access to this important class of materials. As a demonstration of this, we synthesise new **RM734**-like materials in which we vary the number and chemical identity of the lateral and terminal methoxy groups. The methyl-terminated material and, surprisingly, the variant with no terminal chain at all are both competent N_F materials. We report a family of materials with terminal halogen atoms; the iodo-terminated member exhibits the N_F phase whereas others exhibit solely conventional nematic phases. DFT calculations suggest the ability of the iodo-terminated material to form the N_F phase results from the presence of a large Sigma hole on this material enabling a weak electrostatic interaction with the highly electronegative nitro group on an adjacent molecule; effectively making head-to-tail pairing more energetically favourable than with other halogens. The lack of hydrogenolysis conditions in our synthesis permits us to synthesise **RM734**-like materials bearing olefins and unsaturated heterocycles, these would be problematic if not impossible to synthesise with the original synthesis.

Data availability

The data associated with this paper are openly available from the University of Leeds Data Repository at **https://doi.org/10.5518/1411**.

Conflicts of interest

There are no conflicts to declare.

Acknowledgements

R. J. M. acknowledges funding from UKRI *via* a Future Leaders Fellowship, grant no. MR/W006391/1, and funding from the University of Leeds *via* a University Academic Fellowship.

References

1 R. J. Mandle, S. J. Cowling and J. W. Goodby, A Nematic to Nematic Transformation Exhibited by a Rod-like Liquid Crystal, *Phys. Chem. Chem. Phys.*, 2017, **19**, 11429.
2 H. Nishikawa, K. Shiroshita, H. Higuchi, Y. Okumura, Y. Haseba, S. I. Yamamoto, K. Sago and H. Kikuchi, A Fluid Liquid-Crystal Material with Highly Polar Order, *Adv. Mater.*, 2017, **29**, 1702354.
3 X. Chen, *et al.*, First-Principles Experimental Demonstration of Ferroelectricity in a Thermotropic Nematic Liquid Crystal: Polar Domains and Striking Electro-Optics Contributed New Reagents/Analytic Tools; X, *Proc. Natl. Acad. Sci. U. S. A.*, 2002, **117**, 14021.
4 R. J. Mandle, N. Sebastián, J. Martinez-Perdiguero and A. Mertelj, On the Molecular Origins of the Ferroelectric Splay Nematic Phase, *Nat. Commun.*, 2021, **12**, 4962.
5 B. Basnet, M. Rajabi, H. Wang, P. Kumari, K. Thapa, S. Paul, M. O. Lavrentovich and O. D. Lavrentovich, Soliton Walls Paired by Polar Surface Interactions in a Ferroelectric Nematic Liquid Crystal, *Nat. Commun.*, 2022, **13**, 3932.
6 P. Kumari, B. Basnet, H. Wang and O. D. Lavrentovich, Ferroelectric Nematic Liquids with Conics, *Nat. Commun.*, 2023, **14**, 748.
7 O. D. Lavrentovich, Ferroelectric Nematic Liquid Crystal, a Century in Waiting, *Proc. Natl. Acad. Sci. U. S. A.*, 2020, **117**, 14629.
8 X. Chen, E. Korblova, M. A. Glaser, J. E. Maclennan, D. M. Walba and N. A. Clark, Polar In-Plane Surface Orientation of a Ferroelectric Nematic Liquid Crystal: Polar Monodomains and Twisted State Electro-Optics, *Proc. Natl. Acad. Sci. U. S. A.*, 2021, **118**, e2104092118.
9 N. Sebastián, *et al.*, Polarization Patterning in Ferroelectric Nematic Liquids via Flexoelectric Coupling, *Nat. Commun.*, 2023, **14**, 3029.
10 H. Nishikawa, K. Sano, S. Kurihara, G. Watanabe, A. Nihonyanagi, B. Dhara and F. Araoka, Nano-Clustering Mediates Phase Transitions in a Diastereomerically-Stabilized Ferroelectric Nematic System, *Commun. Mater.*, 2022, **3**, 89.
11 J. Li, Z. Wang, M. Deng, Y. Zhu, X. Zhang, R. Xia, Y. Song, Y. Hisai, S. Aya and M. Huang, General Phase-Structure Relationship in Polar Rod-Shaped Liquid Crystals: Importance of Shape Anisotropy and Dipolar Strength, *Giant*, 2022, **11**, 100109.
12 J. Zhou, R. Xia, M. Huang and S. Aya, Stereoisomer Effect on Ferroelectric Nematics: Stabilization and Phase Behavior Diversification, *J. Mater. Chem. C*, 2022, **10**, 8762.
13 C. L. Folcia, J. Ortega, R. Vidal, T. Sierra and J. Etxebarria, The Ferroelectric Nematic Phase: An Optimum Liquid Crystal Candidate for Nonlinear Optics, *Liq. Cryst.*, 2022, **49**, 899.
14 N. Sebastián, R. J. Mandle, A. Petelin, A. Eremin and A. Mertelj, Electrooptics of Mm-Scale Polar Domains in the Ferroelectric Nematic Phase, *Liq. Cryst.*, 2021, **48**, 2055.
15 N. Sebastián, L. Cmok, R. J. Mandle, M. R. De La Fuente, I. Drevenšek Olenik, M. Čopič and A. Mertelj, Ferroelectric-Ferroelastic Phase Transition in a Nematic Liquid Crystal, *Phys. Rev. Lett.*, 2020, **124**, 037801.
16 F. Caimi, G. Nava, R. Barboza, N. A. Clark, E. Korblova, D. M. Walba, T. Bellini and L. Lucchetti, Surface Alignment

of Ferroelectric Nematic Liquid Crystals, *Soft Matter*, 2021, **17**, 8130.

17 H. Nishikawa, K. Sano and F. Araoka, Anisotropic Fluid with Phototunable Dielectric Permittivity, *Nat. Commun.*, 2022, **13**, 1142.

18 S. Nishimura, S. Masuyama, G. Shimizu, C. Chen, T. Ichibayashi and J. Watanabe, Lowering of Electrostatic Actuator Driving Voltage and Increasing Generated Force Using Spontaneous Polarization of Ferroelectric Nematic Liquid Crystals, *Adv. Phys. Res.*, 2022, **1**, 2200017.

19 A. Manabe, M. Bremer and M. Kraska, Ferroelectric Nematic Phase at and below Room Temperature, *Liq. Cryst.*, 2021, **48**, 1079.

20 S. Brown, E. Cruickshank, J. M. D. Storey, C. T. Imrie, D. Pociecha, M. Majewska, A. Makal and E. Gorecka, Multiple Polar and Non-Polar Nematic Phases, *Chem. Phys. Chem.*, 2021, **22**, 2506.

21 R. J. Mandle, Supramolecular Ferroelectric Nematic Materials, *Liq. Cryst.*, 2022, **49**, 2019.

22 R. J. Mandle, A New Order of Liquids: Polar Order in Nematic Liquid Crystals, *Soft Matter*, 2022, **18**, 5014.

23 R. J. Mandle, S. J. Cowling and J. W. Goodby, Structural Variants of RM734 in the Design of Splay Nematic Materials, *Liq. Cryst.*, 2021, **48**, 1780.

24 J. Li, H. Nishikawa, J. Kougo, J. Zhou, S. Dai, W. Tang, X. Zhao, Y. Hisai, M. Huang and S. Aya, Development of Ferroelectric Nematic Fluids with Giant-ε Dielectricity and Nonlinear Optical Properties, *Sci. Adv.*, 2021, **7**, 5047.

25 R. J. Mandle, S. J. Cowling and J. W. Goodby, Rational Design of Rod-Like Liquid Crystals Exhibiting Two Nematic Phases, *Chem. – Eur. J.*, 2017, **23**, 14554.

26 X. Zhao, J. Zhou, J. Li, J. Kougo, Z. Wan, M. Huang and S. Aya, Spontaneous Helielectric Nematic Liquid Crystals: Electric Analog to Helimagnets, *Proc. Natl. Acad. Sci. U. S. A.*, 2021, **118**, e2111101118.

27 N. Tufaha, E. Cruickshank, D. Pociecha, E. Gorecka, J. M. D. Storey and C. T. Imrie, Molecular Shape, Electronic Factors and the Ferroelectric Nematic Phase, *Chem. – Eur. J.*, 2023, **29**, e202300073.

28 E. Cruickshank, R. Walker, J. M. D. Storey and C. T. Imrie, The Effect of a Lateral Alkyloxy Chain on the Ferroelectric Nematic Phase, *RSC Adv.*, 2022, **12**, 29482.

29 D. Pociecha, *et al.*, Intrinsically Chiral Ferronematic Liquid Crystals: An Inversion of the Helical Twist Sense at the Chiral Nematic – Chiral Ferronematic Phase Transition, *J. Mol. Liq.*, 2022, **361**, 119532.

30 M. P. Kumar, J. Karcz, P. Kula, S. Karmakar and S. Dhara, Giant Electroviscous Effects in a Ferroelectric Nematic Liquid Crystal, *Phys. Rev. Appl.*, 2023, **19**, 04408.

31 G. Stepanafas, E. Cruickshank, S. Brown, M. M. Majewska, D. Pociecha, E. Gorecka, J. M. D. Storey and C. T. Imrie, Ferroelectric Nematogens Containing a Methylthio Group, *Mater. Adv.*, 2023, DOI: 10.1039/D3MA00446E.

32 A. D. Becke, Density-Functional Thermochemistry. III. The Role of Exact Exchange, *J. Chem. Phys.*, 1993, **98**, 5648.

33 M. J. Frisch, G. W. Trucks, H. B. Schlegel, G. E. Scuseria, M. A. Robb, J. R. Cheeseman, G. Scalmani, V. Barone, B. Mennucci, G. A. Petersson, H. Nakatsuji, M. Caricato, X. Li, H. P. Hratchian, A. F. Izmaylov, J. Bloino, G. Zheng, J. L. Sonnenberg, M. Hada, M. Ehara, K. Toyota, R. Fukuda, J. Hasegawa, M. Ishida, T. Nakajima, Y. Honda,O. Kitao, H. Nakai, T. Vreven, J. A. Montgomery Jr., J. E. Peralta, F. Ogliaro, M. J. Bearpark, J. Heyd, E. N. Brothers, K. N. Kudin, V. N. Staroverov, R. Kobayashi, J. Normand, K. Raghavachari, A. P. Rendell, J. C. Burant, S. S. Iyengar, J. Tomasi, M. Cossi, N. Rega, N. J. Millam, M. Klene, J. E. Knox, J. B. Cross, V. Bakken, C. Adamo, J. Jaramillo, R. Gomperts, R. E. Stratmann, O. Yazyev, A. J. Austin, R. Cammi, C. Pomelli, J. W. Ochterski, R. L. Martin, K. Morokuma, V. G. Zakrzewski, G. A. Voth, P. Salvador, J. J. Dannenberg, S. Dapprich, A. D. Daniels, Ö. Farkas, J. B. Foresman, J. V. Ortiz, J. Cioslowski and D. J. Fox, *Gaussian 016, Revision E.01*, Gaussian, Inc., Wallingford CT, 2016.

34 S. Grimme, S. Ehrlich and L. Goerigk, Effect of the Damping Function in Dispersion Corrected Density Functional Theory, *J. Comput. Chem.*, 2011, **32**, 1456.

35 R. Saha, P. Nepal, C. Feng, M. S. Hossain, M. Fukuto, R. Li, J. T. Gleeson, S. Sprunt, R. J. Twieg and A. Jákli, Multiple Ferroelectric Nematic Phases of a Highly Polar Liquid Crystal Compound, *Liq. Cryst.*, 2022, **49**, 1784.

36 P. G. M. Wuts and T. W. Greene, *Protection for Phenols and Catechols, in Greene's Protective Groups in Organic Synthesis*, John Wiley & Sons, Ltd, 2006, vol. 4, pp. 367–430.

37 G. Cevasco, G. Guanti, A. R. Hopkins, S. Thea and A. Williams, A Novel Dissociative Mechanism in Acyl Group Transfer from Aryl 4-Hydroxybenzoates in Aqueous Solventst, *J. Org. Chem.*, 1985, **50**, 479.

38 I. H. Um, J. Y. Lee, M. Fujio and Y. Tsuno, Structure-Reactivity Correlations in Nucleophilic Substitution Reactions of Y-Substituted Phenyl X-Substituted Benzoates with Anionic and Neutral Nucleophiles, *Org. Biomol. Chem.*, 2006, **4**, 2979.

39 J. A. Seo, S. I. Kim, Y. J. Hong and I. H. Um, Effect of Alkali Metal Ions on Nucleophilic Substitution Reactions of 4-Nitrophenyl X-Substituted Benzoates with Alkali Metal Ethoxides in Anhydrous Ethanol, *Bull. Korean Chem. Soc.*, 2010, **31**, 303.

40 E. Cruickshank, A. Pearson, S. Brown, J. M. D. Storey, C. T. Imrie and R. Walker, The Ferroelectric Nematic Phase: On the Role of Lateral Alkyloxy Chains, *Liq. Cryst.*, 2023, DOI: 10.1080/02678292.2023.2221651.

41 J. Li, *et al.*, How Far Can We Push the Rigid Oligomers/Polymers toward Ferroelectric Nematic Liquid Crystals?, *J. Am. Chem. Soc.*, 2021, **143**, 17857.

42 D. S. Hulme, E. P. Raynes and K. J. Harrison, Eutectic Mixtures of Nematic 4′-Substitued 4-Cyanobiphenyls, *J. Chem. Soc., Chem. Commun.*, 1974, 98–99.

43 R. J. Mandle, In Silico Interactome of a Room-Temperature Ferroelectric Nematic Material, *Crystals*, 2023, **13**, 857.

44 H. Nishikawa, M. Kuwayama, A. Nihonyanagi, B. Dhara and F. Araoka, Rapid, Solvent-Minimized and Sustainable

Access to Various Types of Ferroelectric-Fluid Molecules by Harnessing Mechano-Chemical Technology, *J. Mater. Chem. C*, 2023, **11**, 12525.

45 J. Y. C. Lim and P. D. Beer, Sigma-Hole Interactions in Anion Recognition, *Chem*, 2018, **4**, 731.

46 L. C. Roper, C. Präsang, V. N. Kozhevnikov, A. C. Whitwood, P. B. Karadakov and D. W. Bruce, Experimental and Theoretical Study of Halogen-Bonded Complexes of DMAP with Di-and Triiodofluorobenzenes. A Complex with a Very Short N···I Halogen Bond, *Cryst. Growth Des.*, 2010, **10**, 3710.